Clim Dyn (2009) 33:917–935
DOI 10.1007/s00382-008-0473-8

Future changes in daily summer temperature variability: driving processes and role for temperature extremes

Erich M. Fischer · Christoph Schär

Received: 20 May 2008 / Accepted: 19 September 2008 / Published online: 14 October 2008

Abstract Anthropogenic greenhouse gas emissions are expected to lead to more frequent and intense summer temperature extremes, not only due to the mean warming itself, but also due to changes in temperature variability. To test this hypothesis, we analyse daily output of ten PRUDENCE regional climate model scenarios over Europe for the 2071–2100 period. The models project more frequent temperature extremes particularly over the Mediterranean and the transitional climate zone (TCZ, between the Mediterranean to the south and the Baltic Sea to the north). The projected warming of the uppermost percentiles of daily summer temperatures is found to be largest over France (in the region of maximum variability increase) rather than the Mediterranean (where the mean warming is largest). The underlying changes in temperature variability may arise from changes in (1) interannual temperature variability, (2) intraseasonal variability, and (3) the seasonal cycle. We present a methodology to decompose the total daily variability into these three components. Over France and depending upon the model, the total daily summer temperature variability is projected to significantly increase by 20–40% as a result of increases in all three components: interannual variability (30–95%), seasonal variability (35–105%), and intraseasonal variability (10–30%). Variability changes in northern and southern Europe are substantially smaller. Over France and parts of the TCZ, the models simulate a progressive warming within the summer season (corresponding to an increase in seasonal variability), with the projected temperature change in August exceeding that in June by 2–3 K. Thus, the most distinct warming is superimposed upon the maximum of the current seasonal cycle, leading to a higher intensity of extremes and an extension of the summer period (enabling extreme temperatures and heat waves even in September). The processes driving the variability changes are different for the three components but generally relate to enhanced land–atmosphere coupling and/or increased variability of surface net radiation, accompanied by a strong reduction of cloudiness, atmospheric circulation changes and a progressive depletion of soil moisture within the summer season. The relative contribution of these processes differs substantially between models.

Keywords Variability · Extreme events · Heat wave

E. M. Fischer (✉) · C. Schär
Universitätstrasse 16, 8092 Zurich, Switzerland
e-mail: erich.fischer@gmail.com

C. Schär
e-mail: schaer@env.ethz.ch

1 Introduction

While summer 2003 was a highly anomalous event even on a seasonal time scale (Schär et al. 2004), most previous European heat waves occurred on substantially shorter scales (e.g. Fischer et al. 2007a). Likewise most of the societal, economical and ecological impacts of heat waves act on daily to weekly time scales. Thus, there is a particular need to understand subseasonal temperature extremes and their sensitivity to changes in mean and daily variability.

Recent observational studies have demonstrated that the frequency of hot summer days and heat waves over Europe has increased in recent decades (e.g. Frich et al. 2002; Klein Tank and Können 2003; Alexander et al. 2006; Tebaldi et al. 2006; Moberg et al. 2006; Della-Marta et al. 2007) along with an enhanced variability of interannual and daily summer temperatures (e.g. Klein Tank et al.

2005; Della-Marta et al. 2007; Scherrer et al. 2008). Over the period 1880 to 2005 the duration of summer heat wave episodes has doubled, the frequency of hot days has almost tripled and the variance of daily temperature has increased by ~6% over western Europe (Della-Marta et al. 2007).

Recent model studies (based on global and regional climate models) have suggested that this trend towards more frequent and intense temperature extremes is very likely to continue and intensify during the 21st century (IPCC 2007, and references therein). Several regional studies found that particularly over a transitional climate zone (TCZ) between the Mediterranean to the south and the Baltic Sea to the north this projected trend is associated with a substantial increase in interannual summer temperature variability (Schär et al. 2004; Rowell 2005; Giorgi and Bi 2005; Clark et al. 2006; Seneviratne et al. 2006; Vidale et al. 2007; Lenderink et al. 2007).

The simulated increase in summer temperature variability also extends to daily time scales, especially over central Europe, where the projected warming is larger for the uppermost percentiles than for the median (Kjellström et al. 2007).

An increase of total daily summer temperature variability may in principle arise from three different reasons: (1) increase in interannual temperature variability, (2) increase in intraseasonal day-to-day variability and (3) increase of the amplitude of the seasonal cycle within summer. The latter component, which will hereafter be referred to as seasonal variability, is often neglected. However, a non-uniform warming within the summer may have a substantial effect on the variability and skewness of the daily temperature distribution as will be shown below. Note that in contrast to other studies our definition of intraseasonal variability excludes the seasonal cycle.

In this study we present a methodology to disentangle the contribution of the aforementioned three components to the total daily summer temperature variability and their role for changes in temperature extremes. Daily output of ten RCM scenario experiments performed within the PRUDENCE project is analysed for the two time slices 1961–1990 and 2071–2100. Projected changes in total daily temperature variability as well as the three contributing components are quantified.

Variability changes on different time scales may be linked to different mechanisms. We investigate the role of different mechanisms acting on interannual and intraseasonal temporal scales with a focus on changes in the surface energy and water budgets.

The mechanisms driving the changes in interannual summer temperature variability relate to a combination of (1) changes in large-scale atmospheric circulation (e.g. Meehl and Tebaldi 2004), as well as small-scale physical processes related to (2) land-surface processes determining the partitioning of latent and sensible heat fluxes (e.g. Seneviratne et al. 2006; Vidale et al. 2007) and (3) cloud effects affecting the surface radiation budget. Land-surface processes are of high importance for extreme events and contributed strongly to the 2003 European heat wave (Fischer et al. 2007b) as well as other recent heat waves (Fischer et al. 2007a). The processes leading to the projected changes on intraseasonal time scales are only poorly investigated.

Changes in variability as well as changes in mean temperature have strong implications for the occurrence of extreme events (Katz and Brown 1992). Using RCM output we demonstrate, how changes in daily statistics of extreme temperatures can be attributed to the different components. Moreover, we investigate how the role of these factors varies between regions.

The paper is structured as follows: in Sect. 2 the PRUDENCE model experiment is summarised. The methodology for the decomposition of the total daily variability into its three components is detailed in Sect. 3. In Sect. 4 the results on the following aspects are presented: (1) variability changes of the different components and the related mechanisms and (2) relevance of the different components for changes in temperature extremes.

2 PRUDENCE multi-model experiment

We use daily output of an ensemble of ten RCM scenario experiments performed within the PRUDENCE project (including nine PRUDENCE standard RCMs and an additional HIRHAM version of the Norwegian Met Office, METNO; see also Jacob et al. 2007). The experiments include control (CTL) simulations of contemporary (1961–1990) climate and scenario (SCN) simulations of future (2071–2100) climate conducted over the European continent. A detailed description of the exact design of the PRUDENCE multi-model experiment is given in Christensen and Christensen (2007), Déqué et al. (2007) and Rowell (2005).

The ten RCMs analysed here are detailed in Table 1. Hereafter we will use the institution name to unambiguously refer to a model version. It is important to note that there are close relationships between some of the models. The HIRHAM simulations conducted at DMI and METNO are performed with the same model applied over different model domains. The ETH and GKSS model share very similar physical parameterisations (same for DMI and MPI model). The ETH and MPI model include the same dynamical core.

The simulations analysed here are all driven with lateral boundary conditions from the HadAM3H atmospheric general circulation model (GCM). In the CTL period the

Table 1 References and characteristics of the regional climate models used in this study

Acronym	Model name	Land surface scheme	Model references
DMI	HIRHAM	ECHAM4 (Düemenil and Todini 1992)	Christensen et al. (1996)
ETH	CHRM	BATS1e (Dickinson et al. 1993)	Vidale et al. (2003)
GKSS	CLM	TERRA LM (Schrodin and Heise 2001)	Steppeler et al. (2003)
HC	HadRM3H	MOSES (Cox et al. 1999)	Buonomo et al. (2007), Jones et al. (1995)
ICTP	RegCM	BATS1e (Dickinson et al. 1993)	Giorgi et al. (1999)
KNMI	RACMO	TESSEL (van den Hurk et al. 2000)	Lenderink et al. (2003)
METNO	HIRHAM-NO	ECHAM4 (Dümenil and Todini 1992)	Hanssen-Bauer et al. (2003)
MPI	REMO	ECHAM4 (Dümenil and Todini 1992)	Jacob (2001)
SMHI	RCAO	RCA2 (Bringfelt et al. 2001)	Döscher et al. (2002), Räisänen et al. (2004)
UCM	PROMES	SECHIBA (Ducoudré et al. 1993)	Castro et al. (1993)

HadAM3H atmospheric GCM is forced with observed monthly fields of sea–surface temperature (SST) and sea-ice extent estimated from observations for current climate. The SSTs for the SCN period are calculated by adding the mean simulated SST changes (differences between 2071–2100 and 1961–1990) to the SSTs of the CTL period (Rowell 2005). These superimposed SST changes (SCN–CTL) are derived from integrations of the coupled atmosphere-ocean global model HadCM3 (Johns et al. 2003) using the IPCC SRES A2 (high emission) scenario (Nakícenovíc et al. 2000).

Almost all RCM simulations analysed were driven with exactly the same lateral boundary conditions and SSTs. The SMHI model is an exception in terms of SSTs and sea ice conditions, as it includes a coupled regional ocean model for the Baltic Sea and Kattegat that internally generates its own SSTs in that area (Döscher et al. 2002; Räisänen et al. 2004). The same SSTs have also been used in the KNMI model. Note that with the ensemble setup used here (one driving GCM) we do not cover the full range of projection uncertainties using the PRUDENCE ensemble, but we are able to isolate the regional response of the surface energy and water budget given virtually identical large-scale forcing.

All models use the same 360-day calendar with a constant month length of 30 days. In general the model domains cover the European continent and parts of the North Atlantic, with some inter-model differences especially in the latitudinal extension (Scandinavia is excluded in UCM and ICTP model, the Iberian Peninsula in METNO). All spatial analyses of daily data were performed on the different native model grids. Regional averages were calculated from land-only gridpoints for the three regions (highlighted in Fig. 2a) Scandinavia (hereafter SC: 55–70°N, 5–30°W), France (FR: 44–50°N, 5°E–5°W), and Iberian Peninsula (IP: 36–44°N, 10°E–3°W). These three subdomains cover the largest differences in zonal characteristics of the variability analysis. The subdomains vary slightly between models because of different grids and land–sea masks. However, given the size of the domains considered, this effect has a negligible influence on the results (see also Frei et al. 2006).

3 Methods

In this section we present a methodology to decompose the total daily summer temperature variability into different components. A difficulty in the estimation of variability is to separate intrinsic variability from trend-induced variability (e.g. Scherrer et al. 2005). The presence of trends in the present temperature series may arise from transient greenhouse-gas forcing or natural variations. Before conducting the decomposition, we thus remove the linear 30-year seasonal summer temperature trends at each grid box and for each 30-year period individually. These linear trends are small during the CTL period (typical range between −0.2 and +0.4 K in 30 years), except for the UCM model, which shows large trends of 1–2 K over some regions. In the SCN period the trends in all models are much larger (typically 1.5–3.5 K in 2071–2100), which results in an considerable trend-induced inflation of the interannual variability (typical inflation factor, ratio of non-detrended to linearly detrended interannual standard deviation of 1.04–1.3). Note that some RCMs show very strong regional trends in the SCN period (e.g. ICTP 4.3 K over Mediterranean or HC 4 K over eastern Europe), which results in substantially larger inflation factors.

The total summer temperature variability σ_{tot} is defined as the standard deviation of all summer daily mean temperatures in a 30-year period, and the variability components considered are: interannual variability (σ'), intraseasonal variability (σ_y''), and variability induced by the summer seasonal cycle ($\hat{\sigma}$). To proceed with the decomposition, the daily mean temperature ($T_{y,d}$) on day d

(of a total of $D = 90$ days) and in year y (of $Y = 30$ years) is expressed as:

$$T_{y,d} = \overline{T} + \hat{T}_d + T'_y + T''_{y,d}, \tag{1}$$

where $\overline{T}$ denotes the 30-year mean summer (JJA) temperature, $\hat{T}_d$ the mean seasonal cycle relative to $\overline{T}$, T_y' the mean summer temperature anomaly in year y, and $T''_{y,d}$ the residual daily anomaly with respect to $\overline{T} + \hat{T}_d + T'_y$ (see Fig. 1 for illustration). The partitioning in Eq. 1 is specifically defined by

$$\hat{T}_d := \frac{1}{Y}\sum_{y=1}^{Y}(T_{y,d} - \overline{T}), \tag{2}$$

$$T'_y := \frac{1}{D}\sum_{d=1}^{D}(T_{y,d} - \overline{T}), \tag{3}$$

and implies $\sum_{d=1}^{D}\hat{T}_d = 0, \sum_{y=1}^{Y}T'_y = 0$, and $\sum_{d=1}^{D}T''_{y,d} = 0$.

Using these three temperature components the total daily variance can be written as

$$\begin{aligned}\sigma^2_{\text{tot}} &= \frac{1}{YD}\sum_{y=1}^{Y}\sum_{d=1}^{D}(T_{y,d} - \overline{T})^2 \\ &= \frac{1}{YD}\sum_{y=1}^{Y}\sum_{d=1}^{D}(\hat{T}_d + T'_y + T''_{y,d})^2.\end{aligned} \tag{4}$$

Similarly, the variance can be expressed for each time component individually as follows: the interannual variance as $\sigma'^2 = \frac{1}{Y}\sum_{y=1}^{Y}T_y'^2$, the variance induced by the seasonal cycle as $\hat{\sigma}^2 = \frac{1}{D}\sum_{d=1}^{D}\hat{T}_d^2$, and the intraseasonal variance in year y as $\sigma''^2_y = \frac{1}{D}\sum_{d=1}^{D}T''^2_{y,d}$. Using these relations, (4) can be rewritten as

$$\sigma^2_{\text{tot}} = \sigma'^2 + \hat{\sigma}^2 + \frac{1}{Y}\sum_{y=1}^{Y}\sigma''^2_y. \tag{5}$$

Above we have used $\hat{T}_d$ (see Eq. 2) to define the mean seasonal cycle, which results in a very noisy signal (due to the small sampling size and the large day-to-day variability). For our analysis we thus use $\tilde{T}_d$ based on a 31-day moving average instead. It is defined as

$$\tilde{T}_d := \frac{1}{31}\sum_{d-15}^{d+15}\frac{1}{Y}\sum_{y=1}^{Y}(T_{y,d} - \overline{T}). \tag{6}$$

The use of $\tilde{T}_d$ instead of $\hat{T}_d$ implies two additional terms in (5), i.e.

$$\begin{aligned}\sigma^2_{\text{tot}} = \sigma'^2 + \tilde{\sigma}^2 + \frac{1}{Y}\sum_{y=1}^{Y}\sigma''^2_y + \frac{2}{Y}\sum_{y=1}^{Y}\left(T'_y\frac{1}{D}\sum_{d=1}^{D}\tilde{T}_d\right) \\ + \frac{2}{D}\sum_{d=1}^{D}\left(\tilde{T}_d\frac{1}{Y}\sum_{y=1}^{Y}T''_{y,d}\right).\end{aligned} \tag{7}$$

Detailed analysis shows that the last two terms in (7) are comparatively small ($<0.01\sigma^2_{\text{tot}}$). The terms are not neglected in the calculation of the results but they are not further discussed since their influence on the variance is very small.

Note that the variance is only a robust measure of scale if the distribution is normally distributed or at least symmetric. The intraseasonal and interannual temperature variability is reasonably symmetric, while the seasonal variability is skewed for some regions. Ferro et al. (2005) have shown that for distributions described by large data samples (e.g. intraseasonal variability) nonparametric quantile-based estimators are more robust measures than parametric approaches. However, for small data samples (e.g. interannual variability) moment-based methods are superior due to their higher statistical efficiency (Scherrer et al. 2005). Here we use the concept of variance to estimate the scale parameters of the individual distributions. This scale estimate is less robust but easily allows us to directly quantify the contribution of the different components (see above). The analysis of the relative changes in intraseasonal and total daily temperature variability (large data samples) have been repeated using robust interquartile range (IQR) estimators as well as skewness (defined as $\frac{1}{DY}\sum_{y=1}^{Y}\sum_{d=1}^{D}(T_{y,d} - \overline{T})^3/\sigma^3_{\text{tot}}$) and have not shown any significant sensitivity.

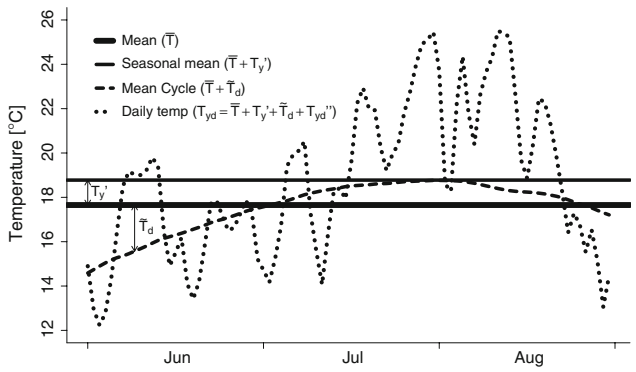

Fig. 1 Illustration of different temperature components used in Eq. 1. See Sect. 3 for details

4 Results

4.1 Changes in total daily variability

In this subsection we analyse simulated changes in the total daily summer temperature variability σ_{tot}, expressed as standard deviations of all summer (JJA) days in 30 years (Fig. 2). The simulated variability in the CTL period is compared to observed variability derived from series of the European Climate Assessment and Dataset project (ECAD)

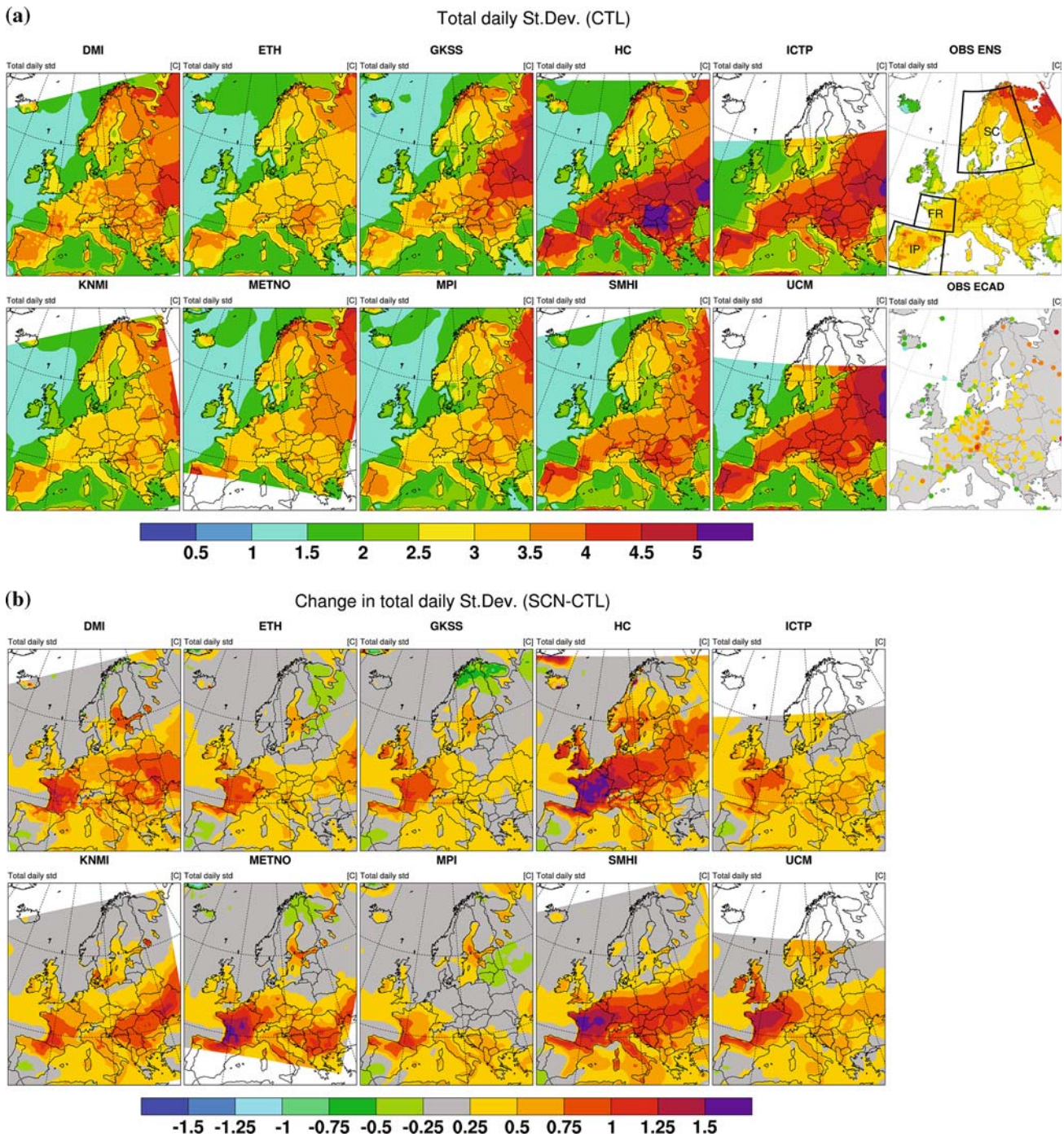

Fig. 2 **a** Total daily temperature variability (K) during summer (JJA) in CTL climate (1961–1990) simulated by ten different regional climate models and derived from the observational ENSEMBLES gridded data and ECAD station series. **b** Simulated change in total daily temperature variability (K) in SCN (2071–2100) wrt CTL

(Klein Tank et al. 2002) and from the gridded ENSEMBLES observational data set (Haylock et al. 2008) for the period 1961–1990. Note that the variability in the model and in ENSEMBLES observational data set is calculated from grid boxes, whereas the variability in the ECAD data is derived from station series. Typically the spatial aggregation over a grid box leads to a somewhat lower variability.

While the majority of the RCMs capture the observed total variability patterns relatively well (Fig. 6a), the HC, ICTP and UCM models overestimated the observed values substantially over the IP, FR and the whole transitional

climate zone (TCZ). The TCZ is defined as the region between the dry Mediterranean climate to the south and the wet climate in the north and refers to the zonal area where evaporation is limited by soil moisture in one summer and not limited in another (see also Seneviratne et al. 2006). At the end of the 21st century all RCMs project strongly enhanced total variability over the TCZ with a pronounced maximum over western Europe (Fig. 2b). Only few models simulate a weak variability decrease over northern Europe and the southern Iberian Peninsula. The pronounced variability increase over western Europe implies more intense temperature extremes over that area. It is remarkable that all RCMs project the strongest increase of the 95th percentile (not shown) over the region of maximum variability increase (mostly France) rather than where the mean warming is largest (southern Europe).

4.2 Changes in interannual variability

The interannual summer temperature variability σ', the standard deviation of the summer (JJA) means, as simulated by the ten PRUDENCE RCMs is depicted in Fig. 3. The comparison against observational data (Fig. 3a) reveals that most models tend to overestimate the interannual summer temperature variability over central and southern parts of Europe. The overestimation is largest over southeastern Europe (too high variability in all RCMs). This may to some extent relate to the summer drying problem of most RCMs (Hagemann et al. 2004) or to circulation biases of the driving GCM HadAM3H (van Ulden et al. 2007). Note the large inter-model differences, especially over central and southern Europe. Over northern Europe all models, except METNO, underestimate the interannual variability.

As regards projected changes in interannual variability (SCN–CTL), Vidale et al. (2007) have shown that in the PRUDENCE ensemble mean, pronounced changes are limited to the boreal summer (JJA), when all ensemble members simulate distinct increases over some portions of the European continent (Fig. 3b). As discussed in Schär et al. (2004), Seneviratne et al. (2006) and Vidale et al. (2007), there are relatively large latitudinal differences in the variability changes. All RCMs show weak variability changes over southern and northern Europe, and almost all RCMs show a very strong increase in the TCZ, which collocates with the strongest gradient in mean summer warming over Europe. Note the considerable inter-model differences in the variability projections over western Europe (largest increase in HC, SMHI and METNO model, smallest in MPI).

Several studies have investigated the mechanisms underlying the increase in summer year-to-year variability in response to greenhouse-gas forcing. Some studies have highlighted the importance of changes in the summer atmospheric circulation (e.g. Meehl and Tebaldi 2004), while others have emphasised the role of land–atmosphere interactions (e.g. Seneviratne et al. 2006; Vidale et al. 2007; Rowell 2005) associated with changes in the surface water and energy budget (Lenderink et al. 2007).

The latter mechanism is related to the projected decrease of the soil water availability over European land regions in response to greenhouse-gas forcing (Wetherald and Manabe 1999; Seneviratne et al. 2002; Rowell and Jones 2006). This effect is also reflected in the PRUDENCE RCMs, which show that in the SCN period the soil moisture reservoirs are accessed earlier in spring (Vidale et al. 2007). This leads to an increased probability of reaching the wilting point and a strong soil moisture control on evapotranspiration (strong land–atmosphere coupling).

Using the ETH model, Seneviratne et al. (2006) identified that soil moisture feedbacks are most relevant for interannual temperature variability in the Mediterranean during the CTL period, but may become a primary driver of the projected variability increase in central and eastern Europe in the SCN period. The role of land–atmosphere coupling for interannual temperature variability is largest in areas where soil moisture is abundant in some summers and strongly limited in others. If soil moisture is strongly limited in every summer (semi-arid climate) or in no summer (wet climate), land–atmosphere interactions play a minor role for interannual variability.

Given abundant soil moisture availability, evapotranspiration and temperature tend to correlate positively, since they both depend on net radiation. However, over regions where the evapotranspiration is controlled by soil moisture availability, there is typically a negative relationship between evapotranspiration and surface temperature (Seneviratne et al. 2006). We here use this relation to identify regions of strong land–atmosphere coupling, where the land surface tends to control the evapotranspiration and thereby affects interannual temperature variability.

Consistent with the ETH model results presented in Seneviratne et al. (2006), most models show a strong anticorrelation of summer mean temperature and evapotranspiration over southern Europe in the CTL period (Fig. 4a). There is a tendency for RCMs with high interannual variability in the CTL period (DMI, HC, MPI, SMHI) to show relatively strong negative correlations. Over northern Europe where evapotranspiration is usually not limited by soil moisture, most RCMs simulate weak positive evapotranspiration-temperature correlations.

In contrast to most of the other RCMs, the UCM model simulates positive correlations over the entire domain, which suggests that temperature in this model is largely controlled by radiation. The fact that the UCM model is

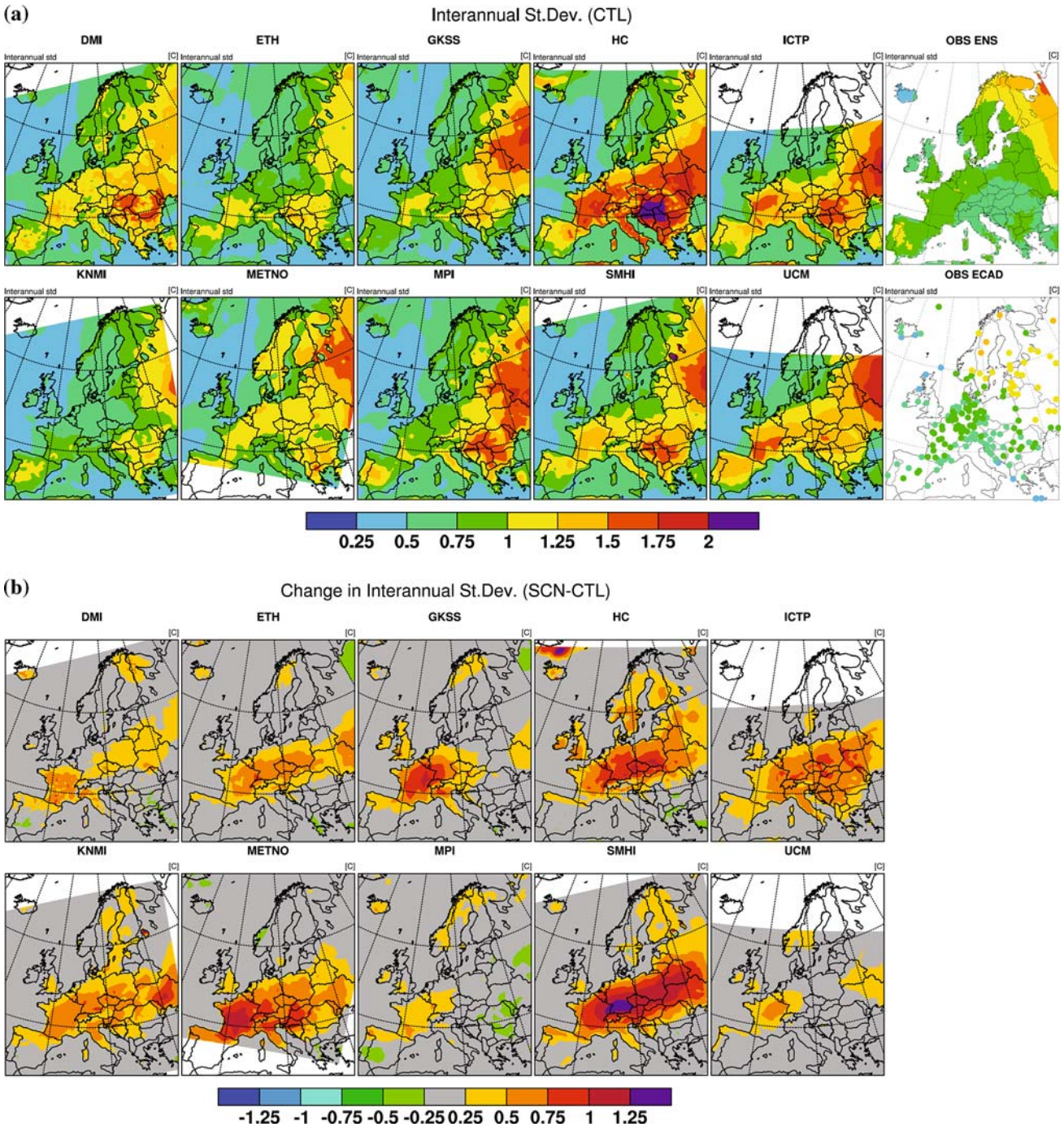

Fig. 3 **a** Interannual summer temperature variability (K) in CTL climate (1961–1990) simulated by ten different regional climate models and derived from the observational ENSEMBLES gridded data and ECAD station series. **b** Simulated change in interannual summer temperature variability (K) in SCN (2071–2100) wrt CTL

rather insensitive to soil drying has been discussed in previous studies, which suggest that it may be linked to too low mean evapotranspiration (Lenderink et al. 2007) and a strong underestimation of the seasonal soil-moisture cycle (Hirschi et al. 2007).

As regards climate change most RCMs predict a substantial northward shift of the region with strongest land–atmosphere coupling in the SCN period (Fig. 4b). In the majority of the analysed RCMs the anticorrelations in SCN period are enhanced especially over the TCZ (area of largest temperature variability increase). Four RCMs show a somewhat different behaviour. The MPI and UCM models, which project only a weak interannual temperature variability increase, show only a moderate (MPI) or no

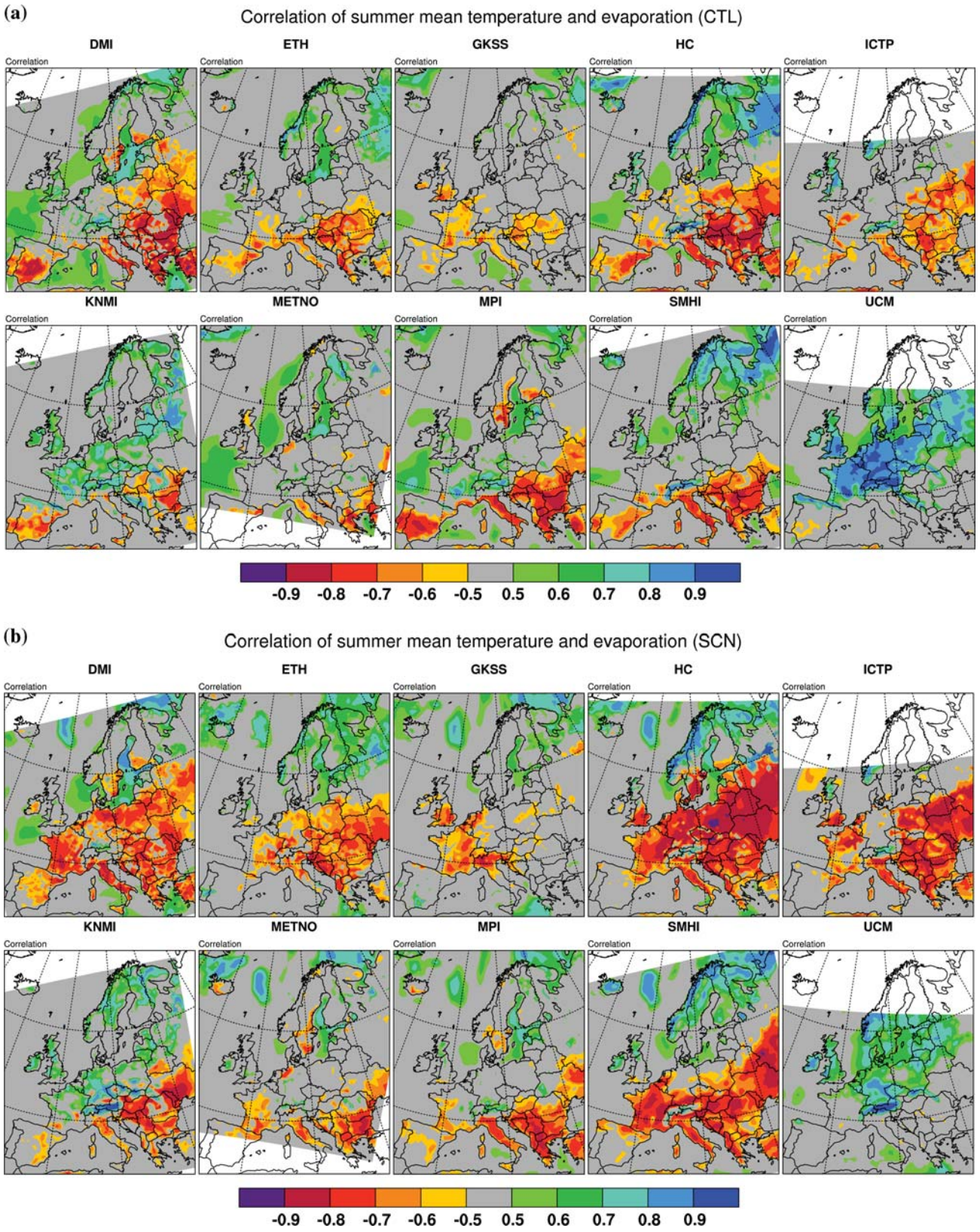

Fig. 4 Gridpoint correlation of mean summer temperature and evapotranspiration in **a** CTL (1961–1990) and **b** SCN period (2071–2100) in different regional climate models

change (UCM) of land–atmosphere coupling. However, also the KNMI and GKSS model, which both project a strong increase of interannual variability, show only a weak intensification of land–atmosphere coupling. This suggests that different mechanisms may partly control the variability increase in these two models.

Figure 5 shows that KNMI and GKSS simulate a strong increase in interannual surface net radiation variability, which collocates with the enhanced interannual temperature variability. This suggests that in contrast to the other models, the increase in net radiation variability is the main driving mechanism in these two RCMs. Thus, depending on the model the interannual temperature variability increase is mainly driven by land–atmosphere coupling or radiative processes (associated with atmospheric circulation variability and cloud processes) or a combination of the two, with differing contributions depending on the region.

These findings are consistent with Lenderink et al. (2007) who suggest that the short-wave radiation is the dominant factor in some RCMs, whereas in others the effect of evapotranspiration is most important. In the former case cloud feedbacks are essential, whereas in the latter soil-moisture feedbacks are the crucial processes.

Over the southern IP, where the interannual temperature variability is projected to remain unchanged or to decrease, all RCMs except the ICTP model simulate a substantial weakening of the land–atmosphere coupling (Fig. 4b). We suggest that over this region, the soil moisture regularly reaches the wilting point under greenhouse-gas induced summer drying, as also reflected by the absence of any significant interannual summer soil-moisture variability in the SCN period (not shown). Consequently, summer temperatures are no longer sensitive to soil moisture.

4.3 Changes in intraseasonal variability

The intraseasonal summer temperature variability ($\sigma_y''^2$, see definition in Sect. 3) is a measure of the amplitude of daily variations around the seasonal cycle ($\tilde{T}$). Generally the intraseasonal variability is small over oceans and along coasts, and comparatively large over land regions (Fig. 6a).

In order to validate the simulated intraseasonal variability, the ten CTL simulations are compared against observations from ECAD station data and the gridded ENSEMBLES data set (Haylock et al. 2008). Most of the RCMs are in relatively good agreement with observed values across Europe (Fig. 6a). As for the total variability, the HC, ICTP and UCM models tend to overestimate the intraseasonal variability over the northern IP and the TCZ.

According to Fig. 6b all RCMs show a general tendency towards higher intraseasonal variability in the SCN period

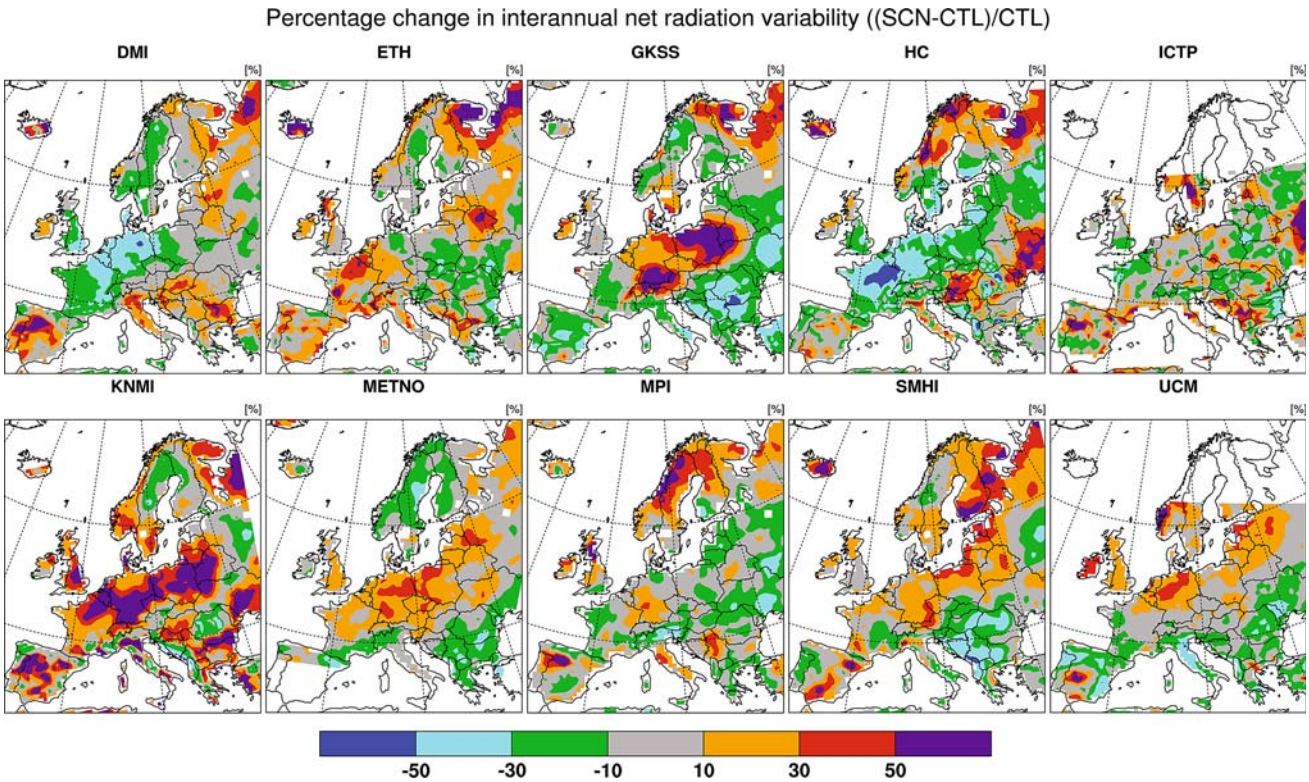

Fig. 5 Percentage change in interannual variability of mean summer net surface radiation between CTL (1961–1990) and SCN (2071–2100) period

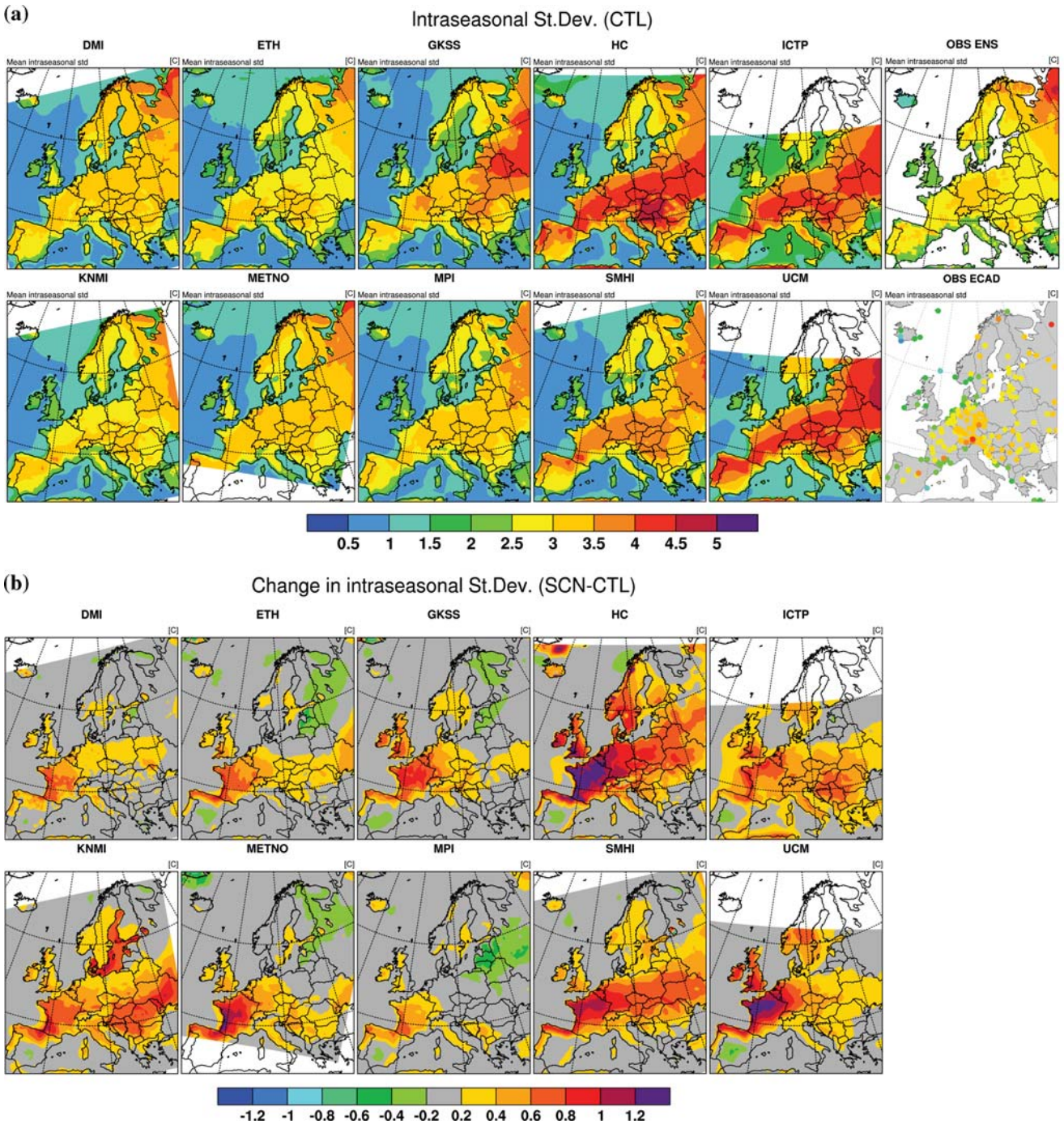

Fig. 6 **a** Intraseasonal summer temperature variability (K) in CTL (1961–1990) simulated by ten different regional climate models and derived from the observational ENSEMBLES gridded data and ECAD station series. **b** Simulated change in intraseasonal summer temperature variability (K) in SCN (2071–2100) wrt CTL

(2071–2100) in particular over the TCZ. Most RCMs simulate the maximum increase over FR (0.5–1.5 K), further west than in the case of interannual variability. Over northern Europe and the southern IP, some models project a small reduction of intraseasonal variability. A detailed analysis of the latter region revealed that in the SCN period the intraseasonal temperature distribution has a very short-tailed maximum (see later in Fig. 10), in contrast to most other regions. The distinct upper bound of the distribution is presumably constrained by the temperature maximum reached, when virtually all of the available net radiation is converted into sensible heat due to lack of soil moisture.

The definitions of interannual and intraseasonal variability are independent (cf. Sect. 3). Nevertheless there is a

tendency for RCMs with high (low) intraseasonal variability to simulate high (low) interannual variability, especially over central and southern Europe. This may be related to similar processes, parameterisations and model characteristics, which are relevant for variability on both time scales (see following discussion of mechanisms).

In all RCMs the intraseasonal day-to-day variations are highly dependent on synoptic variability and associated cloud cover, and are highly correlated with surface shortwave and net radiation. However, the models do not simulate any future increase in shortwave and total net radiation variability, which would explain the increase in intraseasonal temperature variability. In contrary there is even a slight decrease in intraseasonal net radiation variability primarily over southern Europe (not shown).

Soil moisture variations have a comparatively low frequency and hence cannot directly account for day-to-day temperature variations. However, the enhanced future summer drying results in a general reduction of evapotranspiration (found to be strongest over western Europe) and this implies enhanced sensible heat fluxes in most RCMs. The efficacy of this indirect effect is confirmed by the fact that some RCMs show a tendency to higher intraseasonal variability in warm and dry years. In addition, the soil drying implies a lower heat capacity of the soil, such that the day-to-day temperature variations become more susceptible to intraseasonal net radiation variability.

4.4 Changes in seasonal cycle and implied variability

In this subsection we analyse the temperature variability induced by the seasonal cycle ($\tilde{T}$) and its future changes. A more pronounced seasonal cycle, which implies larger temperature contrasts within the summer, would enhance the seasonal variability $\tilde{\sigma}$ and thereby also σ_{tot}. Furthermore, changes in the seasonal cycle may also affect the shape (skewness) of the daily temperature distribution.

Over the IP (Fig. 7a) and SC (Fig. 7c) the greenhouse-gas induced warming is rather uniform within the summer (JJA). However, over FR (Fig. 7b) and other areas within the TCZ, the warming differs substantially between early and late summer (typically 2–3 K more warming in August

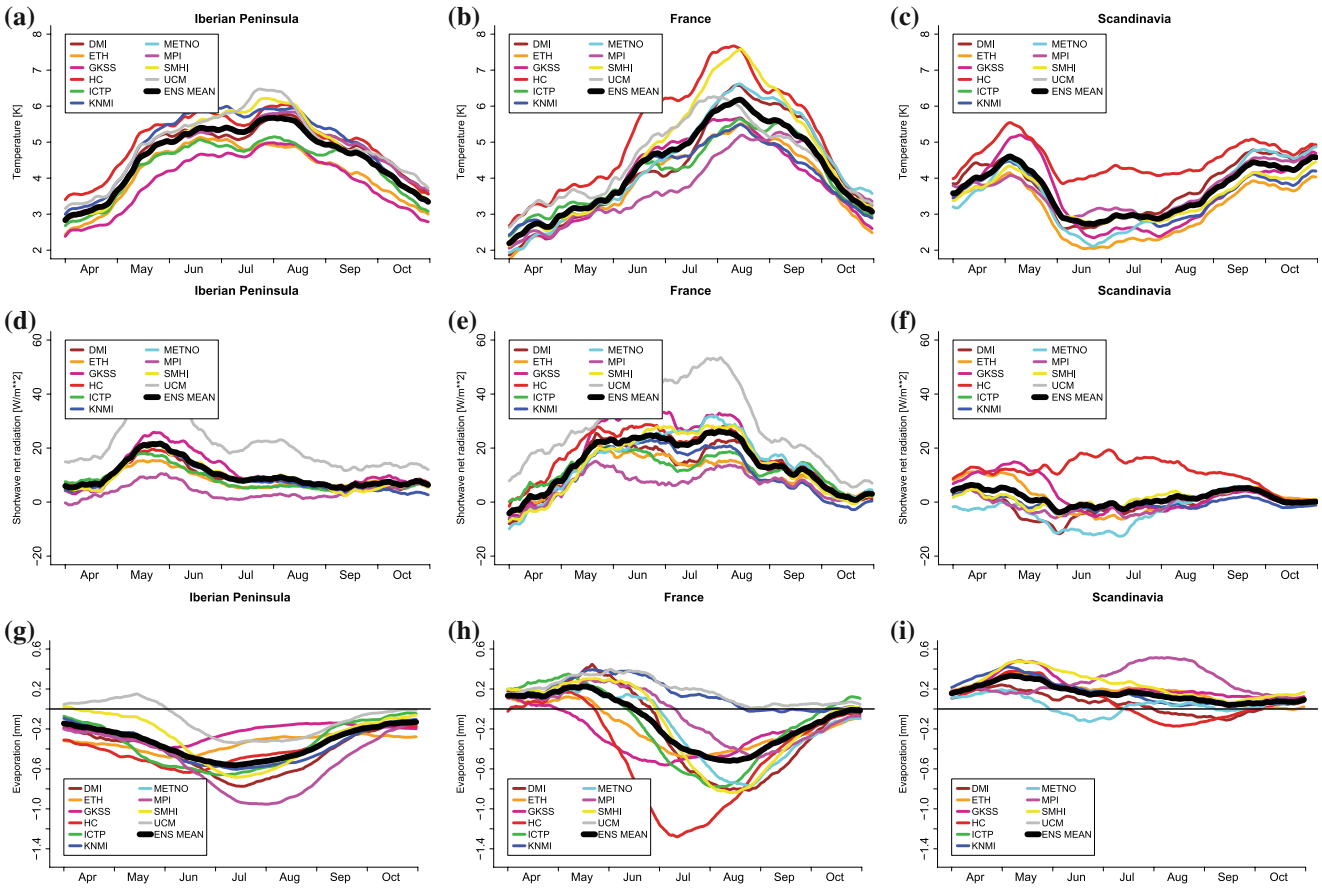

Fig. 7 Changes in mean seasonal cycle $(\overline{T}_{\mathrm{SCN}} + \tilde{T}_{\mathrm{SCN}}) - (\overline{T}_{\mathrm{CTL}} + \tilde{T}_{\mathrm{CTL}})$ of (**a**–**c**) temperature, (**d**–**f**) shortwave net surface radiation, and (**g**–**i**) evapotranspiration simulated by ten different regional climate models for the regions (**a**, **d**, **g**) Iberian Peninsula, (**b**, **e**, **h**) France, and (**c**, **f**, **i**) Scandinavia. The seasonal cycle is defined as a 31-day moving average

than in June). The future increase in the associated standard deviation $\tilde{\sigma}$ amounts to typically 30–100% (ensemble mean change 53%) over FR (Fig. 8d).

A progressive warming within the summer may also shift the timing of the maximum temperature of the seasonal cycle and favour heat waves to occur earlier or later than in the CTL period. Under current climatic conditions the maximum temperatures are reached between mid-July (northern Europe) and early August (southern Europe).

In FR, the maximum warming is simulated for early to mid-August and is thereby superimposed to almost the hottest period in the current summer climate. This implies particularly pronounced summer peak temperatures in the future, a tendency to postponed culmination of the seasonal temperature cycle, and also an elongation of the summer period into the autumn. Over FR, September temperatures in SCN reach values around or higher than July temperatures in CTL. This suggests that in the future, heat waves of

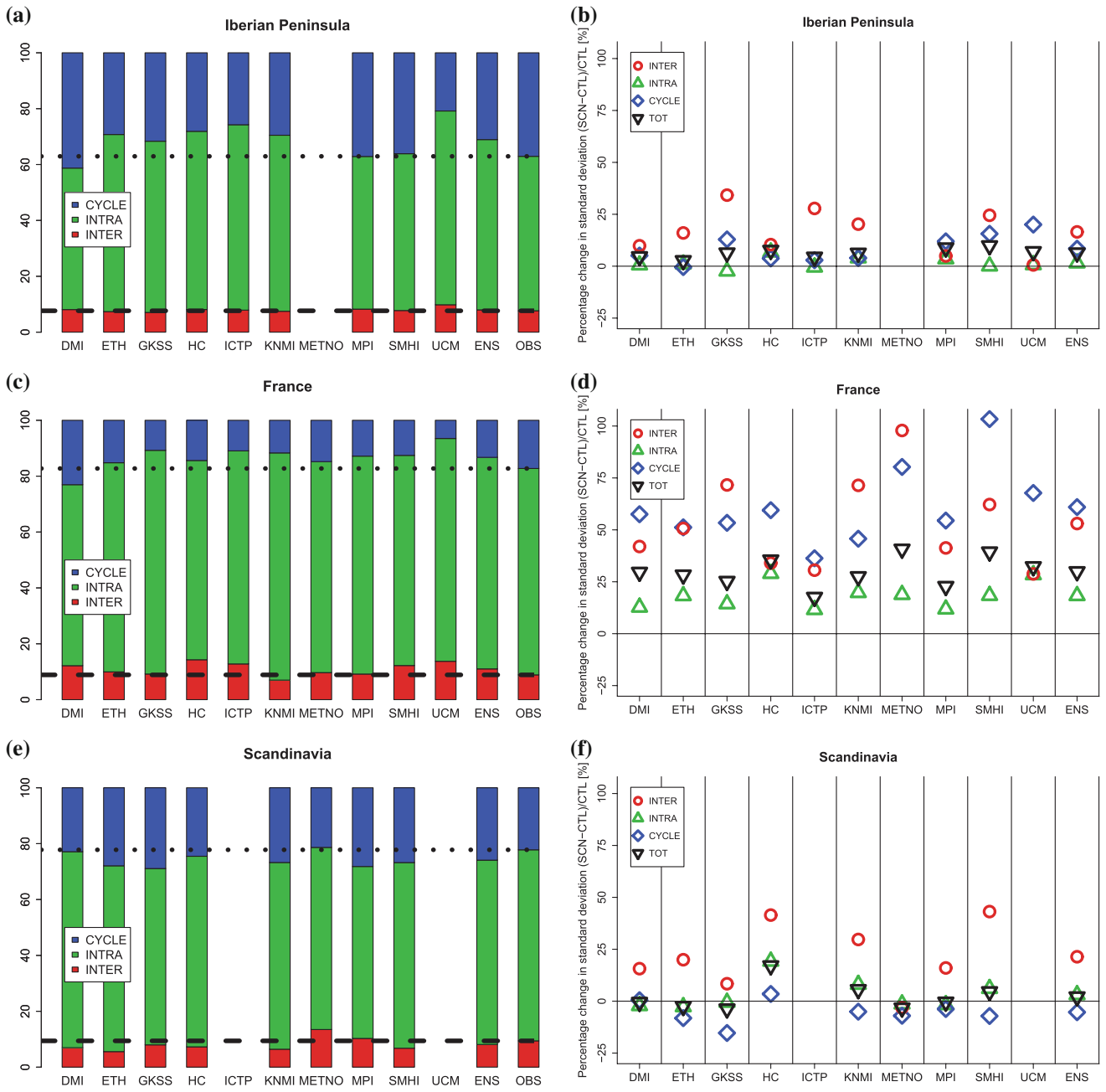

Fig. 8 **a**, **c**, **e** Contribution (%) of the three components to the total daily variance σ^2_{tot} in CTL as simulated by ten different regional climate models and the ensemble mean (ENS). The *rightmost bar* and the *dashed/dotted lines* depict the same percentages calculated from the ENSEMBLES gridded observational data set. **b**, **d**, **f** Percentage change in the total daily standard deviations and its three components computed as [(SCN–CTL)/CTL]. Ensemble mean change is shown in *rightmost section*

the magnitude as they currently occur in July may become possible even during early September.

We suggest that the mechanism causing the aforementioned progressive summer warming is mainly related to land-surface processes. The warming at the end of summer is amplified by the progressive soil drying. This effect is also reflected in the reduced evapotranspiration in late summer, which shows the largest negative difference (SCN–CTL) during the same period as the maximum warming (Fig. 7h). Note that there are very large differences between RCMs, which are mainly related to different soil properties and land surface parameterisations (cf discussion in Sect. 4.2). Moreover, van Ulden et al. (2007) revealed a tendency towards more easterly circulation types during summer in SCN. The frequency of easterlies, which is correlated with higher summer temperatures, increases particularly in late summer, which adds to the progressive summer warming. The projected increase in shortwave net radiation is relatively uniform within the summer (Fig. 7e) and cannot explain the progressive warming within summer.

Over the IP, the warming (SCN–CTL) reaches a maximum already in May and remains uniform thereafter (Fig. 7a). We suggest that this is due to the anomalously strong net radiation in early summer and due to the earlier start of the soil-moisture controlled limitation of evapotranspiration.

Over SC, the projected summer warming is relatively uniform and smaller than during the other seasons. The summer warming in SC is mainly controlled by radiative processes and advection, whereas changes in land–atmosphere feedbacks are expected to play a minor role.

4.5 Contribution of variability components to daily total variability

In the previous subsections we have shown that the total daily temperature variability and its three components—interannual, intraseasonal and seasonal variability—are projected to increase over most of the regions. In order to quantify the relative contribution of the components, the total daily variance is expressed as

$$\frac{\sigma'^2}{\sigma_{\mathrm{tot}}^2}+\frac{\tilde{\sigma}^2}{\sigma_{\mathrm{tot}}^2}+\frac{\frac{1}{Y}\sum_{y=1}^{Y}\sigma''^2}{\sigma_{\mathrm{tot}}^2}\simeq 1. \quad (8)$$

Since we here calculate the seasonal cycle $\tilde{T}$ based on a moving time window (and not on daily basis, $\hat{T}$), this expression does not exactly equal 1 (see Sect. 3). However, the difference corresponds to generally less than 0.01. In the CTL period the intraseasonal variance explains by far the largest portion of the total variance (about 50–80%, see left-hand panels of Fig. 8). The interannual variance corresponds to typically 8–10% and the seasonal variance to 10–40%. These percentages compare well with observations (ENSEMBLES gridded data) shown in the rightmost bar.

As regards climate change, the relative increase of total daily standard deviation σ_{tot} [(SCN–CTL)/CTL] varies between the different regions (ensemble mean change 6% over IP, 30% over FR, 2% over SC; see black triangles in Fig. 8 right-hand panels). Note that given the large sample size the total variability changes larger than 5% are significant at the 99% confidence level. While the changes in all variability components are rather small over SC and IP, they are highly significant over FR (Fig. 8d) and the entire TCZ (not shown). Note that in the case of interannual variability, not all RCMs project changes that are significant (too small sample size of 30 years). Over FR, interannual and seasonal variability increase substantially stronger than intraseasonal variability (Fig. 8d). The magnitude of the simulated changes differs between RCMs, especially for $\tilde{\sigma}$ and σ', while the changes in σ_{tot} and σ'' are relatively robust.

These findings indicate a growing relative contribution of interannual variance over FR, associated with larger differences between individual summers. The increased contribution of the seasonal cycle points to a more important role of the differences between the beginning of the summer and the hottest period in late July/early August. However, overall the intraseasonal variance confirms to have a dominant contribution in all regions even in the future. Note that an analysis of the variability changes based on IQR instead of σ, which is not documented in this paper for brevity, led to virtually the same results, except for the interannual temperature distribution (IQR non-robust due to small sample size).

4.6 Sensitivity of extremes to changes in variability components

We have shown that greenhouse-gas induced climate change is expected to enhance the total summer temperature variability over large parts of Europe. Here, we discuss the implications of these variability changes for the frequency and intensity of summer temperature extremes. In order to quantify changes in temperature extremes, we analyse the widely used extreme indices T90f and T95f, which are defined as the frequency of exceedance of the 90th/95th percentile of the daily climatology (CTL). For validation the CTL distribution is compared against the observed distribution (ENSEMBLES data set). While the general shape of the daily temperature distribution in FR (Fig. 9) and IP (Fig. 10) is well captured, there are considerable mean biases in some RCMs. The IQR is

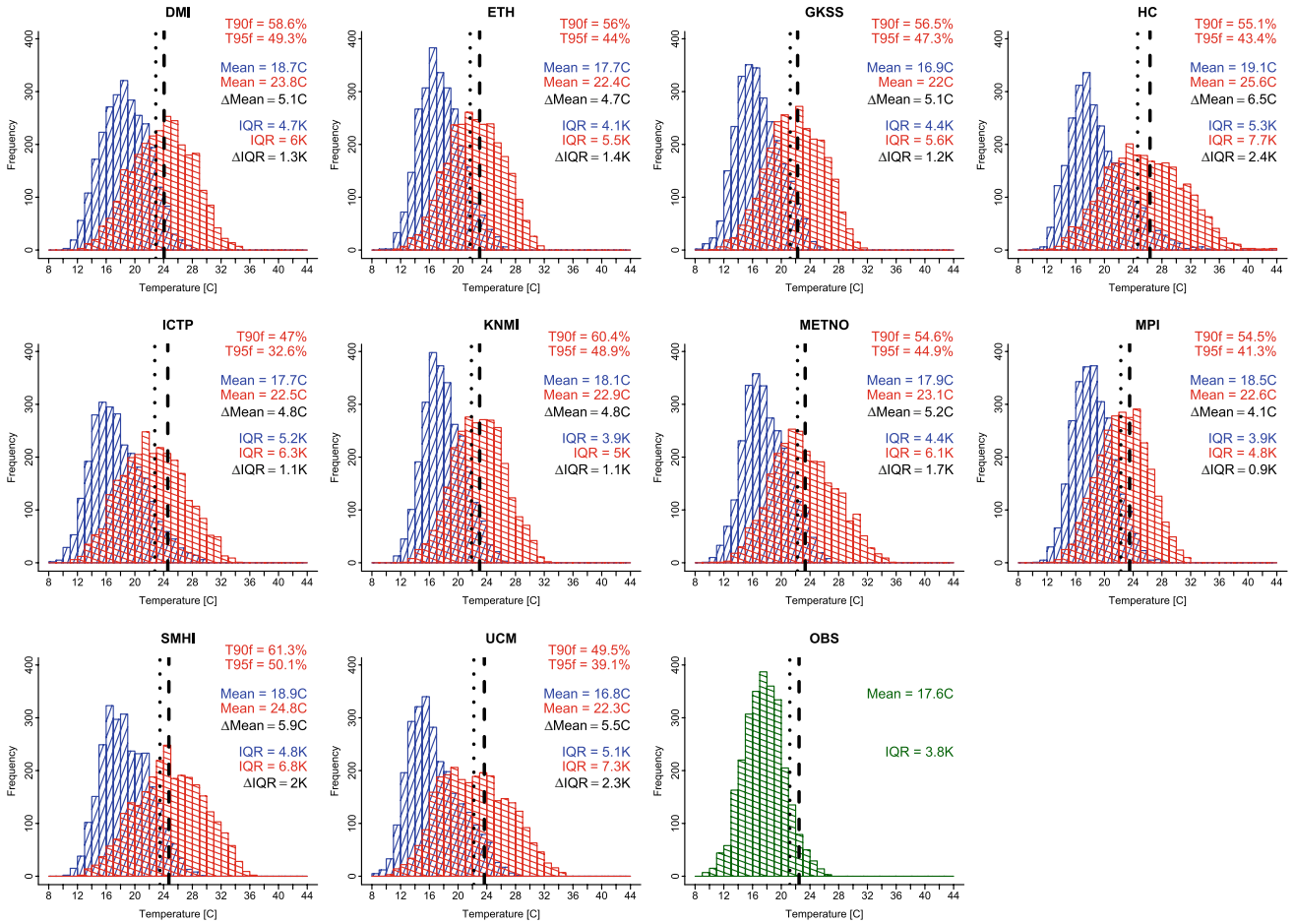

Fig. 9 Daily temperature distribution in CTL (1961–1990, *blue*) and SCN (2071–2100, *red*) simulations over France (number of summer days in a 30-year period). The observed temperature distribution (1961–1990) from the ENSEMBLES observational data set is shown in the *last panel in green*. The 90th and 95th percentiles relative to the respective CTL distributions are marked by *dotted* and *dashed lines*, respectively

overestimated in all RCMs in FR and relatively well captured over the IP.

T90f and T95f are projected to increase over all European regions, with strong (weak) changes over southern (northern) Europe. Over FR, T95f amounts to typically 30–50% in SCN compared to 5% in CTL (Fig. 9). Thus for the SRES scenario considered, at least every second to third summer day exceeds the 95th percentile, and a considerable number of days even the maximum values of the CTL period. T90f and T95f would be even higher, if May and September were included in the analysis of SCN. Note that the strongest increase in T90f and T95f is not simulated by those RCMs that show the largest mean warming.

In the following, we illustrate the contribution of the mean warming and variability increase to changes in temperature extremes over FR (Fig. 11) using the example of the ETH model, which in CTL shows good agreement with the observed temperature distribution.

Figure 11b visualises the consequences of mean warming only on T90f and T95f. The fact that T90f amounts to 55.5% and T95f to 39.2% in the absence of any change in variability, manifests the dominant role of the change in the mean. As pointed out by Barnett et al. (2006) and Clark et al. (2006), the change in mean principally captures most of the change in the percentile exceedance. However, it is important to note that in most RCMs the warming of the uppermost percentiles is largest over FR (strongest variability increase) and not over the IP (strongest mean warming), which points to an important role of variability changes for the most extreme values.

The variability changes have strong implications particularly near the tails of the distribution. In the absence of a mean change, T90f and T95f would amount to 15.7 and 8%, respectively (Fig. 11c). Note that the changes are more apparent in the cold tail because the CTL distribution is strongly positively skewed. The influence of interannual variability alone is illustrated in Fig. 11d by upscaling of

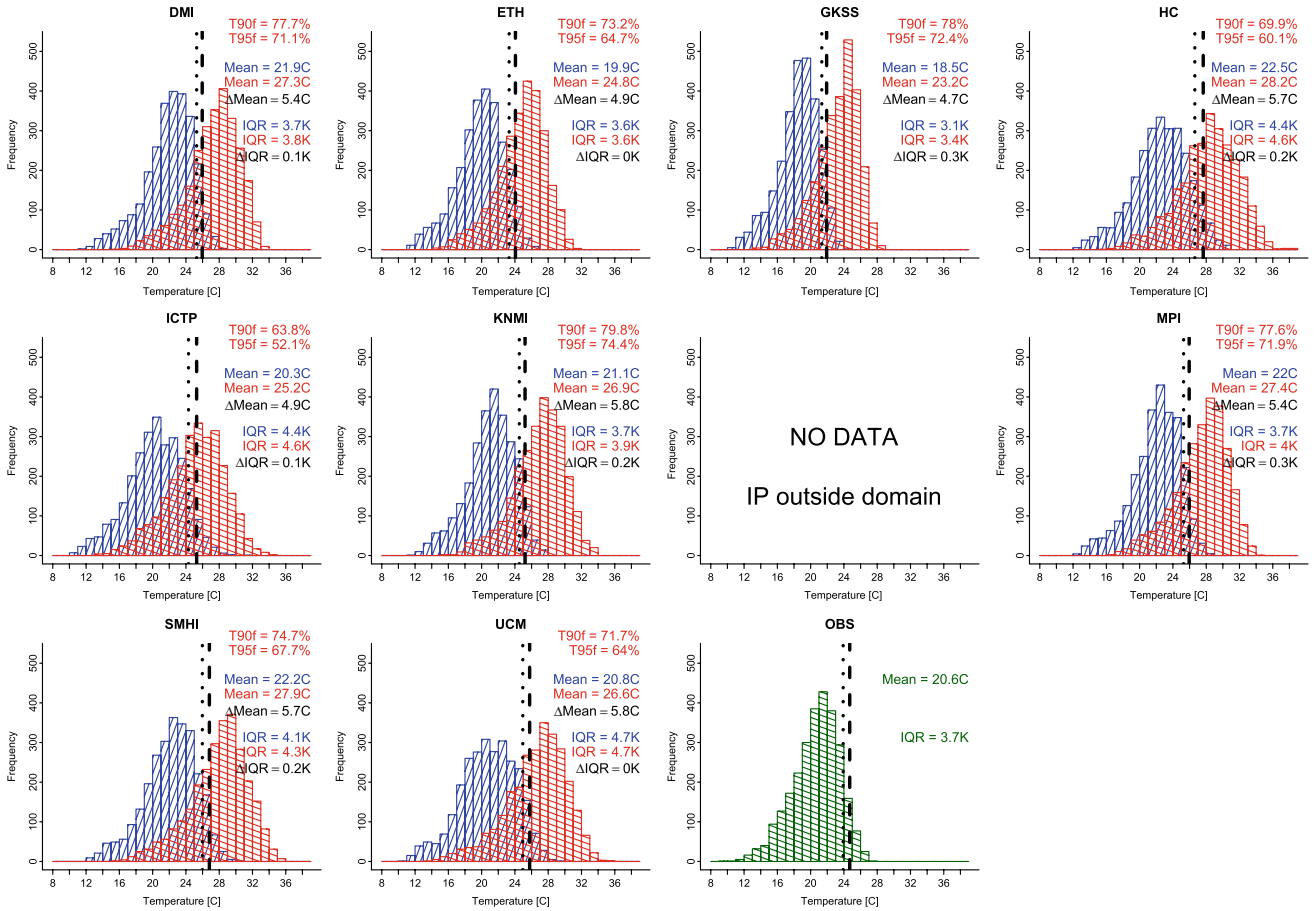

Fig. 10 Same as Fig. 9 but for Iberian Peninsula

the seasonal mean anomalies of CTL such as to reach the same interannual standard deviation as in SCN. This results in a moderate increase of T90f and T95f and a pronounced change at the tails of the distribution. Changes in intra-seasonal variability have a very strong effect on the IQR and result in a substantial increase of T90f (Fig. 11e). Furthermore, there is a pronounced change in the skewness of the distribution, which is also affected by the change in the cycle (Fig. 11f). Moreover, changes in the seasonal cycle result in a moderate increase of T90f and T95f. Note that the exact contribution of the variability components differs significantly between regions and is considerably larger for some RCMs.

Over IP the increase of T90f and T95f is substantially larger (Fig. 10) with T95f reaching 50–75% in the SCN period. This is mainly due to the larger mean warming over IP compared to FR. The change in variability is rather small over IP and hence plays a secondary role for the changes in T90f and T95f. However, due the pronounced negative skewness in both the CTL and SCN period (see also observed temperatures), the same mean shift has a much stronger effect on the threshold exceedance than in other regions.

As mentioned above, the short upper tail (negative skewness) is mainly the result of the seasonal cycle with relatively cool temperatures in early June and constantly high temperatures in July and August. However, even if the seasonal cycle is removed, there is a tendency to a negatively skewed temperature distribution over the IP. We suggest that the distinct upper bound is determined by the available net radiation on clear-sky days, when converted into sensible heating under conditions of dry soils.

5 Summary and conclusions

We have analysed daily output of ensemble scenario experiments performed with ten regional climate models over Europe for the periods 1961–1990 and 2071–2100 driven by an SRES A2 greenhouse-gas scenario. All models predict a strong warming as well as considerable changes in the variability of daily summer temperatures. The projected changes in total daily temperature variability (standard deviation of all summer days in 30-year period) differ substantially between RCMs and show a characteristic latitudinal dependence. A pronounced variability

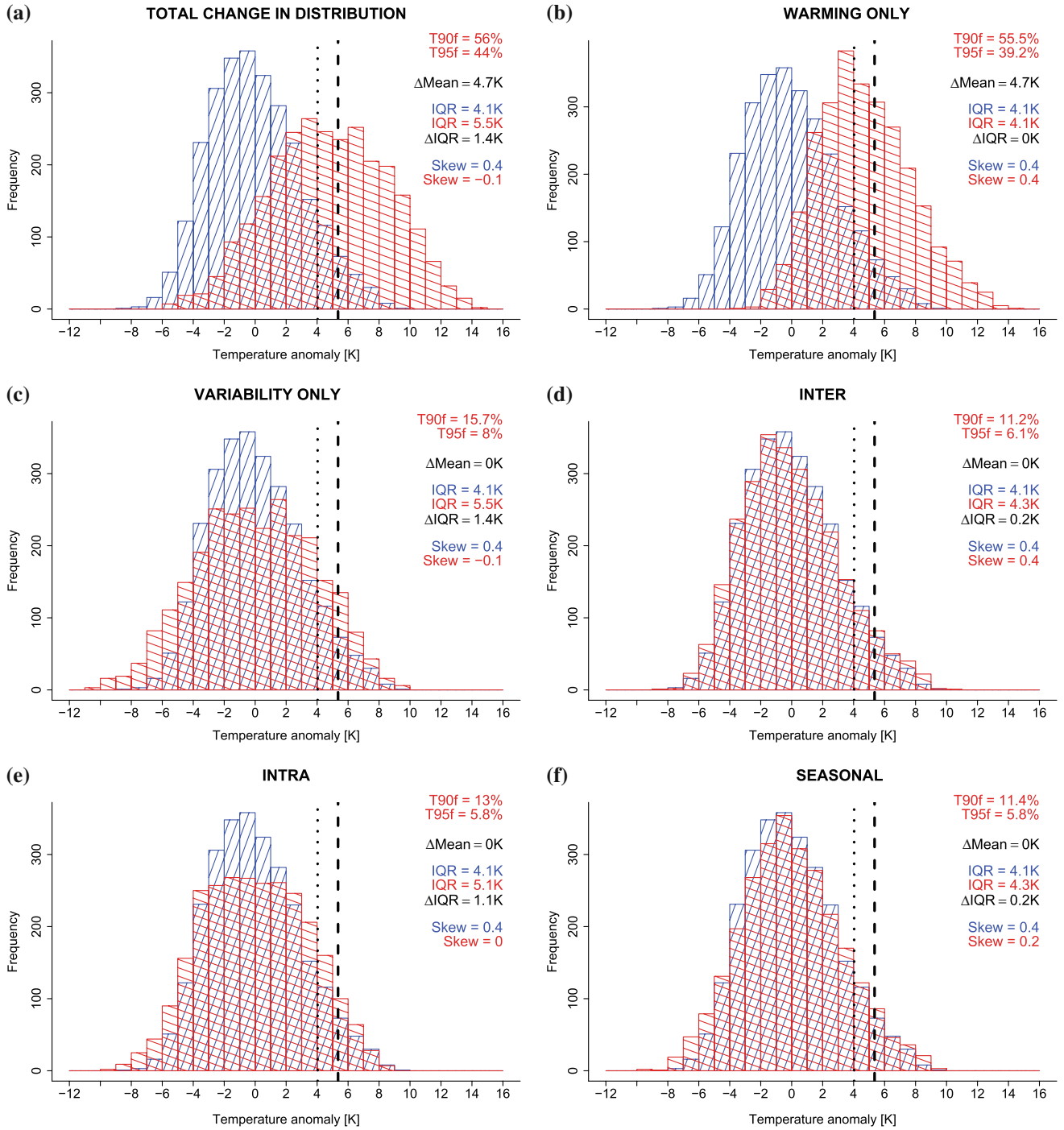

Fig. 11 Role of different components for the daily temperature distribution changes over France between CTL (1961–1990) and SCN (2071–2100) as simulated by the ETH model: **a** total simulated change, **b** simulated change due to mean warming only, **c** variability change only (without mean warming), **d** due to changes in interannual variability only, **e** due to changes in intraseasonal variability only, **f** due to changes in seasonal variability only. For the definition of skewness see Sect. 3

increase is simulated over the TCZ between the Baltic Sea to the north and the Mediterranean to the south. Over France and depending upon the model, the total daily temperature variability increases by 20–40%. Changes in northern and southern Europe are substantially smaller.

The projected changes in daily temperature variability arise from changes of its three time components: interannual, intraseasonal and seasonal variability. We have presented a method to decompose the total variability into its three components. Note that in contrast to other studies

the intraseasonal variability does not include variability induced by the seasonal cycle, which is analysed separately as seasonal variability.

The variability of all three components increases particularly over the aforementioned TCZ. Over France and depending upon the model, the interannual variability increases by 30–95%, the seasonal variability by 35–105%, and the intraseasonal variability by 10–30%. As a result of these changes, the relative importance of interannual and seasonal variability grows at the expense of intraseasonal variability.

The seasonal variability increases due to a non-uniform warming within the summer. Over France, there is a progressive summer warming, which is typically 2–3 K larger in August than in June. This suggests that the strongest warming within summer is superimposed upon the highest temperatures of the current climate, with a slight tendency to a postponed culmination of the temperature cycle. Likewise, our simulations suggest an elongated summer period, with September temperatures (SCN) reaching values around or higher than July temperatures in CTL. This indicates that in the future, heat waves of the magnitude as they currently occur in July may become possible even during early September.

As regards the driving processes, the non-uniform warming arises mainly from the amplifying effect of dry soils in late summer. The mechanism underlying the increase in interannual variability is to a large extent due to the growing importance of land–atmosphere coupling and enhanced net surface radiation variability. The roles of these two mechanisms varies substantially between models and regions. The projected intraseasonal variability increase mainly relates to the strong soil drying, which limits latent cooling and reduces the surface heat capacity. Thus, the same intraseasonal net radiation variability translates into larger intraseasonal temperature variability.

The aforementioned changes have strong implications for the frequency and intensity of temperature extremes. Maximum changes are projected for southern Europe, where the frequency of hot summer days (defined using a local 95-percentile CTL threshold) increases from 5% in CTL to about 65% in SCN. In the TCZ between the Mediterranean to the south and the Baltic Sea to the north, the frequency of hot summer days increases from 5 to about 40%. A large portion of the increased frequency of hot days arises from the strong mean summer warming, especially over southern Europe. However, in addition the increase in total daily temperature variability strongly affects the tails of the distribution. This is supported by the fact that in most RCMs the warming of the uppermost percentiles is largest over France (strongest variability increase) and not over the Iberian Peninsula (strongest mean warming).

This study suggests an increasing risk of summer temperature extremes along with a mean warming and enhanced temperature variability on interannual, seasonal and daily time scales. In particular the changes in short-term temperature variations deserve close attention, since most of the societal, economical and ecological impacts of heat waves act on daily and weekly time scales.

References

Alexander L, Zhang X, Peterson T, Caesar J, Gleason B, Tank AK, Haylock M, Collins D, Trewin B, Rahimzadeh F, Tagipour A, Kumar K, Revadekar J, Griffiths G, Vincent L, Stephenson D, Burn J, Aguilar E, Brunet M, Taylor M, New M, Zhai P, Rusticucci M, Vazquez-Aguirre J (2006) Global observed changes in daily climate extremes of temperature and precipitation. J Geophys Res 111

Barnett DN, Brown SJ, Murphy JM, Sexton DMH, Webb MJ (2006) Quantifying uncertainty in changes in extreme event frequency in response to doubled CO_2 using a large ensemble of GCM simulations. Clim Dyn 26. doi:10.1007/s00382-005-0097-1

Bringfelt B, Räisänen J, Gollvik S, Lindström G, Graham LP, Ullerstig A (2001) The land surface treatment for the Rossby centre regional atmospheric climate model version 2 (RCA2). Reports meteorology and climatology, vol 98, Swedish Meteorological and Hydrological Institute, Norrköping

Buonomo E, Jones R, Huntingford C, Hannaford J (2007) On the robustness of changes in extreme precipitation over Europe from two high resolution climate change simulations. Q J R Meteorol Soc 133:65–81

Castro M, Fernández C, Gaertner M (1993) Mathematics, climate and environment. Description of a meso-scale atmospheric numerical model

Christensen JH, Christensen OB (2007) A summary of the PRUDENCE model projections of changes in European climate by the end of this century. Clim Change 81:7–30

Christensen J, Christensen OB, Lopez P, van Meijgaard E, Botzet M (1996) The HIRHAM4 regional atmospheric climate model. Technical report, DMI Technical Report 96-4

Clark RT, Brown SJ, Murphy JM (2006) Modeling Northern hemisphere summer heat extreme changes and their uncertainties using a physics ensemble of climate sensitivity experiments. J Clim 19:4418–4435

Cox PM, Betts RA, Bunton CB, Essery RLH, Rowntree PR, Smith J (1999) The impact of new land surface physics on the GCM simulation of climate and climate sensitivity. Clim Dyn 15:183–203

Della-Marta PM, Luterbacher J, Weissenfluh HV, Xoplaki E, Brunet M, Wanner H (2007) Doubled length of Western European summer heat waves since 1880. J Geophys Res 112. doi:10.1029/2007JD008510

Déqué M, Rowell D, Schär C, Giorgi F, Christensen JH, Rockel B, Jacob D, Kjellström E, de Castro M, van den Hurk B (2007) An intercomparison of regional climate models for Europe: assessing uncertainties in model projections. Clim Change 81:53–70

Dickinson R, Henderson-Sellers A, Kennedy P (1993) Biosphere-atmosphere transfer scheme (BATS) version le as coupled to the NCAR community climate model, NCAR technical note

Döscher R, Willén U, Jones C, Rutgersson A, Meier H, Hansson U, Graham L (2002) The development of the regional coupled ocean-atmosphere model RCAO. Boreal Environ Res 7:183–192

Ducoudré NI, Laval K, Perrier A (1993) SECHIBA, a new set of parameterizations of the hydrologic exchanges at the land–atmosphere interface within the LMD atmospheric general circulation model. J Clim 6:248–273

Dümenil L, Todini E (1992) A rainfall-runoff scheme for use in the Hamburg climate model. In: O'Kane JP (ed) Advances in theoretical hydrology. A tribute to James Dooge. European geophysical society series on hydrological sciences, vol 1. Elsevier, Amsterdam, pp 129–157

Ferro CAT, Hannachi A, Stephenson DB (2005) Simple nonparametric techniques for exploring changing probability distributions of weather. J Clim 18:4344–4354

Fischer EM, Seneviratne SI, Lüthi D, Schär C (2007a) Contribution of land–atmosphere coupling to recent European summer heat waves. Geophys Res Lett 34. doi:10.1029/2006GL029068

Fischer EM, Seneviratne SI, Vidale PL, Lüthi D, Schär C (2007b) Soil moisture-atmosphere interactions during the 2003 European summer heat wave. J Clim 20:5081–5099

Frei C, Schöll R, Fukutome S, Schmidli J, Vidale PL (2006) Future change of precipitation extremes in Europe: intercomparison of scenarios from regional climate models. J Geophys Res 111. doi:10.1029/2005JD005965

Frich P, Alexander L, Della-Marta P, Gleason B, Haylock M, Tank A, Peterson T (2002) Observed coherent changes in climatic extremes during the second half of the twentieth century. Clim Res 19:193–212

Giorgi F, Bi X (2005) Regional changes in surface climate interannual variability for the 21st century from ensembles of global model simulations. Geophys Res Lett 32. doi:10.1029/2005GL023002

Giorgi F, Huang Y, Nishizawa K, Fu C (1999) A seasonal cycle simulation over eastern Asia and its sensitivity to radiative transfer and surface processes. J Geophys Res 104:6403–6423

Hagemann S, Machenhauer B, Jones R, Christensen O, Déqué M, Jacob D, Vidale PL (2004) Evaluation of water and energy budgets in regional climate models applied over Europe. Clim Dyn 23:547–567. doi:10.1007/s00382-004-0444-7

Hanssen-Bauer I, Førland E, Haugen J, Tveito O (2003) Temperature and precipitation scenarios for Norway: comparison of results from dynamical and empirical downscaling. Clim Res 25:15–27

Haylock M, Hofstra N, Klein Tank A, Klok E, Jones P, New M (2008) A European daily high-resolution gridded dataset of surface temperature and precipitation for 1950–2006. J Geophys Res (in press)

Hirschi M, Seneviratne SI, Hagemann S, Schär C (2007) Analysis of seasonal terrestrial water storage variations in regional climate simulations over Europe. J Geophys Res 112. doi:10.1029/2006JD008338

IPCC (2007) Climate change 2007: the physical science basis. In: Contribution of working group I to the fourth assessment report of the Intergovernmental Panel on Climate Change. Cambridge University Press, Cambridge, 996 pp

Jacob D (2001) A note to the simulation of the annual and inter-annual variability of the water budget over the Baltic Sea drainage basin. Meteorol Atmos Phys 77:61–73

Jacob D, Bärring L, Christensen OB, Christensen JH, de Castro M, Déqué M, Giorgi F, Hagemann S, Hirschi M, Jones R, Kjellström E, Lenderink G, Rockel B, Sanchez E, Schär C, Seneviratne SI, Somot S, van Ulden A, van den Hurk B (2007) An inter-comparison of regional climate models for Europe: model performance in present-day climate. Clim Change 81:31–52

Jones R, Murphy J, Noguer M (1995) Simulation of climate change over Europe using a nested regional climate model I: assessment of control climate, including sensitivity to location of lateral boundaries. Q J R Meteorol Soc 121:1413–1449

Johns TC, Gregory JM, Ingram WJ, Johnson CE, Jones A, Lowe JA, Mitchell JFB, Roberts DL, Sexton DMH, Stevenson DS, Tett SFB, Woodage MJ (2003) Anthropogenic climate change for 1860 to 2100 simulated with the HadCM3 model under updated emissions scenarios. Clim Dyn 20. doi:10.1007/s00382-002-0296-y

Katz RW, Brown BG (1992) Extreme events in a changing climate: variability is more important than averages. Clim Change 21:289–302

Kjellström E, Bärring L, Jacob D, Jones R, Lenderink G, Schär C (2007) Modelling daily temperature extremes: recent climate and future changes over Europe. Clim Change 81:249–265

Klein Tank A, Wijngaard J, Können G, Böhm R, Demarée G, Gocheva A, Mileta M, Pashiardis S, Hejkrlik L, Kern-Hansen C, Heino R, Bessemoulin P, Muller-Westermeier G, Tzanakou M, Szalai S, Palsdottir T, Fitzgerald D, Rubin S, Capaldo M, Maugeri M, Leitass A, Bukantis A, Aberfeld R, Engelen AV, Forland E, Mietus M, Coelho F, Mares C, Razuvaev V, Nieplova E, Cegnar T, Lopez J, Dahlström B, Moberg A, Kirchhofer W, Ceylan A, Pachaliuk O, Alexander L, Petrovic P (2002) Daily dataset of 20th-century surface air temperature and precipitation series for the European climate assessment. Int J Climatol 22:1441–1453

Klein Tank A, Können G, Selten F (2005) Signals of anthropogenic influence on European warming as seen in the trend patterns of daily temperature variance. Int J Climatol 25:1–16

Klein Tank AMG, Können GP (2003) Trends in indices of daily temperature and precipitation extremes in Europe, 1946–99. J Clim 16:3665–3680

Lenderink G, van den Hurk B, van Meijgaard E, van Ulden A, Cujipers H (2003) Simulation of present-day climate in RACMO2: first results and model developments. KNMI technical report

Lenderink G, van Ulden A, van den Hurk B, van Meijgaard E (2007) Summertime inter-annual temperature variability in an ensemble of regional model simulations: analysis of the surface energy budget. Clim Change 81:233–247

Meehl GA, Tebaldi C (2004) More intense, more frequent, and longer lasting heat waves in the 21st century. Science 305:994–997

Moberg A, Jones P, Lister D, Walther A, Brunet M, Jacobeit J, Alexander L, Della-Marta P, Luterbacher J, Yiou P, Chen D, Tank A, Saladie O, Sigro J, Aguilar E, Alexandersson H, Almarza C, Auer I, Barriendos M, Begert M, Bergstrom H, Bohm R, Butler C, Caesar J, Drebs A, Founda D, Gerstengarbe F, Micela G, Maugeri M, Osterle H, Pandzic K, Petrakis M, Srnec L, Tolasz R, Tuomenvirta H, Werner P, Linderholm H, Philipp A, Wanner H, Xoplaki E (2006) Indices for daily temperature and precipitation extremes in Europe analyzed for the period 1901–2000. J Geophys Res 111. doi:10.1029/2006JD007103

Nakícenovíc N, Alcamo J, Davis G, de Vries B, Fenhann J, Gaffin S, Gregory K, Grübler A, Jung T, Kram T, La Rovere E, Michaelis L, Mori S, Morita T, Pepper W, Pitcher H, Price L, Riahi K, Roehrl A, Rogner H-H, Sankovski A, Schlesinger M, Shukla P, Smith S, Swart R, van Rooijen S, Victor N, D. Z (2000) A special report of working group III of the Intergovernmental Panel on Climate Change. Cambridge University Press, Cambridge

Räisänen J, Hansson U, Ullerstig A, Döscher R, Graham L, Jones C, Meier H, Samuelsson P, Willén U (2004) European climate in the late twenty-first century: regional simulations with two driving global models and two forcing scenarios. Clim Dyn 22:13–31

Rowell DP (2005) A scenario of European climate change for the late twenty-first century: seasonal means and interannual variability. Clim Dyn 25:837–849

Rowell DP, Jones RG (2006) Causes and uncertainty of future summer drying over Europe. Clim Dyn 27:281–299

Schär C, Vidale PL, Lüthi D, Frei C, Häberli C, Liniger MA, Appenzeller C (2004) The role of increasing temperature variability in European summer heatwaves. Nature 427:332–336. doi:10.1038/nature02300

Scherrer SC, Appenzeller C, Liniger MA, S. C (2005) European temperature distribution changes in observations and climate change scenarios. Geophys Res Lett 32. doi:10.1029/2005GL024108

Scherrer SC, Liniger M, Appenzeller C (2008) Climate variability and extremes during the past 100 years. In: Distribution changes of seasonal mean temperature in observations and climate change scenarios. Advances in global change research, vol 33. Springer, Heidelberg, 390 pp

Schrodin R, Heise E (2001) The multi-layer version of the DWD soil model TERRALM. Technical report 2, COSMO

Seneviratne SI, Pal JS, Eltahir EAB, Schär C (2002) Summer dryness in a warmer climate: a process study with a regional climate model. Clim Dyn 20:69–85. doi:10.1007/s00382-002-0258-4

Seneviratne SI, Lüthi D, Litschi M, Schär C (2006) Land–atmosphere coupling and climate change in Europe. Nature 443:205–209

Steppeler J, Doms G, Schattler U, Bitzer H, Gassmann A, Damrath U, Gregoric G (2003) Meso-gamma scale forecasts using the nonhydrostatic model LM. Meteorol Atmos Phys 82:75–96

Tebaldi C, Hayhoe K, Arblaster J, Meehl G (2006) Going to the extremes. Clim Change 79:185–211

van den Hurk BJJM, Viterbo P, Beljaars ACM, Betts AK (2000) Offline validation of the ERA40 surface scheme. Tech memo 295, ECMWF, Reading

van Ulden A, Lenderink G, van den Hurk B, van Meijgaard E (2007) Circulation statistics and climate change in central Europe: PRUDENCE simulations and observations. Clim Change 81:179–192

Vidale PL, Lüthi D, Frei C, Seneviratne SI, Schär C (2003) Predictability and uncertainty in a regional climate model. J Geophys Res 108. doi:10.1029/2002JD002810

Vidale PL, Lüthi D, Wegmann R, Schär C (2007) European summer climate variability in a heterogeneous multi-model ensemble. Clim Change 81:209–232

Wetherald RT, Manabe S (1999) Detectability of summer dryness caused by greenhouse warming. Clim Change 43:495–511